Nanostructure and Nanomechanics of Cement: Polydisperse Colloidal Packing

E. Masoero,[1] E. Del Gado,[2] R. J.-M. Pellenq,[1,3] F.-J. Ulm,[1] and S. Yip[4]

[1]*Department of Civil and Environmental Engineering, Massachusetts Institute of Technology, Cambridge, Massachusetts 02139, USA*
[2]*Department of Civil, Environmental and Geomatic Engineering, ETH Zürich, 8093 Zurich, Switzerland*
[3]*CINaM, CNRS and Aix-Marseille University, Campus de Luminy, 13288 Marseille Cedex 09, France*
[4]*Department of Nuclear Science and Engineering, Massachusetts Institute of Technology, Cambridge, Massachusetts 02139, USA*

(Received 6 December 2011; revised manuscript received 23 March 2012; published 10 October 2012)

Cement setting and cohesion are governed by the precipitation and growth of calcium-silicate-hydrate, through a complex evolution of microstructure. A colloidal model to describe nucleation, packing, and rigidity of calcium-silicate-hydrate aggregates is proposed. Polydispersity and particle size dependent cohesion strength combine to produce a spectrum of packing fractions and of corresponding elastic properties that can be tested against nanoindentation experiments. Implications regarding plastic deformations and reconciling current structural characterizations are discussed.

DOI: 10.1103/PhysRevLett.109.155503 PACS numbers: 62.25.−g, 62.20.D−, 82.70.Dd

The cohesive strength of concrete arises from the hardening of cement paste, produced by mixing cement powder with water (hydration) and allowing time for setting. Hydration and setting encompass dissolution and precipitation at the molecular scale, growth of hydration products up to the micron scale, and rigidity percolation through micron to millimeter size cement powder grains [1,2]. The mechanics of cement setting is believed to be governed by the properties of the hydration product calcium-silicate-hydrate (C-S-H), which forms a nanoporous highly cohesive phase, that glues together the different components. While controlling the development of the C-S-H structure and its subsequent evolution is clearly the key to advance cement technology, it is still fundamentally not known how the mesoscale organization develops, from the nanometer scale to the stress-bearing submicron structure, and how this determines the mechanical behavior of the cement paste [1].

The nature of C-S-H itself is elusive and complex. Recent studies suggest that during the precipitation of hydration products, C-S-H clusters aggregate on the nanoscale, due to net attractive electrostatic forces, giving rise to a colloidal type of gel already at relatively low densities [3,4]. This evolves, during setting, into a dense mature microstructure, whose nanoscale mechanics is suggestive of a jammed packed assembly of rigid grains [5], which also indicates a highly heterogeneous structure in terms of local density. Within this scenario, there is a need to elucidate the interplay between cohesive interactions and packing, in analogy to colloidal gels and glasses [6,7].

We study C-S-H precipitation and aggregation using a primitive model of space filling of cohesive nanoscale, colloidal units. Previous works [3,4,8] support such simplification, in order to capture the underlying *physical* mechanisms. We show that this approach can span length scales from nanometer sized C-S-H aggregates up to mesoscale sub-micron organization. Using Monte Carlo simulations, we calculate the elastic moduli measured in nanoindentation tests and obtain results in the same range as existing experiments. We demonstrate the experimentally observed wide range of C-S-H local densities can be associated with the polydispersity of the C-S-H aggregates, formed during dissolution and precipitation. Furthermore, our study clarifies the role of the polydispersity of C-S-H clusters, as well their strong cohesive interactions. Our results support the idea that C-S-H is akin to a very heterogeneous medium, an amorphous strongly cohesive solid with dynamical features typical of slowly evolving, aging glassy materials. Within this picture, local irreversible structural rearrangements could manifest in a granular-type of mechanical response, as the one observed in nanoindentation tests [5,9].

We model an open system of C-S-H particles with a uniform size distribution, from a minimum σ_m to a maximum σ_M value. Among other possible definitions (see, e.g., Ref. [10]), we choose the standard deviation δ of the initial distribution in units of $1/2(\sigma_M + \sigma_m)$ as the measure of polydispersity. The nature of effective interactions in C-S-H is still a subject of intensive investigation, as experiments and atomistic simulations suggest a narrow attractive potential would be appropriate [11]. We adopt a generalized Lennard-Jones form for particle interactions:

$$U_{ij}(r_{ij}) = 4\varepsilon(\bar{\sigma}_{ij})\left[\left(\frac{\bar{\sigma}_{ij}}{r_{ij}}\right)^{2\gamma} - \left(\frac{\bar{\sigma}_{ij}}{r_{ij}}\right)^{\gamma}\right], \qquad (1)$$

where r_{ij} is the interparticle distance, $\varepsilon(\bar{\sigma}_{ij})$ is the well depth between two particles with different size σ_i and σ_j, and $\bar{\sigma}_{ij} = (\sigma_i + \sigma_j)/2$. The potential minimum is at $r_{ij} = r_m = \sqrt[6]{2}\bar{\sigma}_{ij}$, while the maximum attractive force dU_{ij}/dr_{ij} occurs at $r_{ij} = r_u = \sqrt[\gamma]{2 + 2\gamma/(\gamma + 1)}\bar{\sigma}_{ij}$, with rupture strain $(r_u - r_m)/r_m$ independent of $\bar{\sigma}_{ij}$. Assuming $\varepsilon(\bar{\sigma}_{ij}) \propto \sigma_{ij}^3$, which is equivalent to taking the Young's modulus Y to be uniform over the system [12], then the unit pressure $\varepsilon(\bar{\sigma}_{ij})/\bar{\sigma}_{ij}^3$ is a constant. As a result, mechanical

 © 2012 American Physical Society

quantities with dimension of force per unit area become scale invariant, for example the specific energy, the pressure, the strength, and the elastic moduli. We parametrize the interaction potential in Eq. (1) to describe the physical properties of the hydration product C-S-H. We have in mind mature C-S-H aggregates, because our simulation results will be tested against experiment data at advanced stages of setting. In such conditions, the tensile rupture strain of zero-porosity C-S-H is $\approx 5\%$, and its Young modulus is 72.5 GPa [11,13]. This gives $\gamma = 14$ and $Y = 72.5$ GPa [14]. In spite of the very deep well, we are still able to observe significant local rearrangements of small size particles, about 1 nm, due to thermal fluctuations [15]. On the other hand, the steep increase of ϵ with σ^3 makes already particles with $\sigma < 10$ nm behave as practically athermal.

The precipitation of C-S-H microstructures is simulated by successively and randomly inserting particles into an initially empty cubic periodic simulation cell. We use a Metropolis algorithm with probability of insertion $P_{\text{acc}} = \min[1, e^{-\Delta U/(k_B T)}]$. ΔU is the difference in interaction energy after and before insertion, k_B is the Boltzmann constant, and $T = 298$ K is the temperature [16]. Between successive insertion attempts, a delay is introduced to allow for structural relaxation in the NVT ensemble. The delay consists of $1/R_p$ Monte Carlo displacements, with R_p being the precipitation rate. The insertion procedure is terminated when the number of particles inside the simulation cell converges to a maximum value determined by the space filling. Thus the particle configuration and corresponding packing fraction produced through this procedure reflect the combined effects of relaxation under strong cohesive interactions, and rate-dependent space filling. We examine monodisperse ($\delta = 0$) and polydisperse C-S-H clusters up to $\delta = 0.47$ (i.e., $\sigma_M/\sigma_m = 10$). The range of particle size considered lies between 1 and 10 nm. The total number of Monte Carlo trials for the formation process ranges between 10^8 and 2×10^{10}, the precipitation rate R_p between 1 and 10^{-6}, the simulation cell size between $6.8\sigma_m$ and $40\sigma_m$, and the final number of particles between 300 and 12 000.

Results.—Figure 1(a) shows a typical configuration obtained at the end of our simulation of C-S-H microstructure formation. Space filling progressively disfavors the insertion of large particles, and the final particle size distributions (PSDs) deviate appreciably from the initial uniform distribution. The resulting PSDs can be well described by geometric distributions $p(\sigma) = \alpha\sigma^{\alpha-1}/(\sigma_M^\alpha - \sigma_m^\alpha)$, also known to be optimal for packing hard spheres [17]. We find α depends significantly on R_p; namely, a small R_p leads to a greater number of large particles. This seems physically reasonable in that small R_p favors particle flocculation between two successive insertions, creating wider voids to accommodate large particles [16]. The systems at the termination of insertion are in tension because of strong interparticle attractions, and because structural rearrangements are carried out under NVT condition. In order to compare our results with experiments on mature C-S-H specimens at ambient pressure, we relax the microstructure by decreasing the simulation cell dimensions via NPT ensemble, down to a volume V_0. Because our unit of pressure has a high value, $\epsilon(\bar{\sigma}_{ij})/\bar{\sigma}_{ij}^3 = 0.204$ GPa (from Ref. [14]), atmospheric pressure is effectively zero in our model. Figure 1(b) shows that the obtained packing fraction $\phi_0 = V_0^{-1}\sum_{i=1}^{N} 1/6(\sqrt[14]{2}\sigma_i)^3$ starts at a value around random close packing (0.64) for a monodisperse system and increases nonlinearly with the polydispersity δ. The same trend is seen in molecular dynamics simulations of jamming polydisperse hard spheres [18]. This points to a certain generality of how polydispersity affects packing fractions. ϕ_0 depends very weakly on the insertion rate R_p and therefore on the shape factor α of the PSD, within the range of parameters explored here. This result differs from those regarding hard spheres, where ϕ can depend significantly on α [17]. We also find the specific cohesive energy $\sum U_{ij}/V_0$ at zero pressure is weakly dependent on R_p and consequently on α. All this suggests that interactions and relaxation to zero pressure play a central role in our study. We will return to this discussion below.

We evaluate the elastic properties of the relaxed microstructures, by computing the full 4th order elastic tensor using the stress fluctuation method [19], and assessing mechanical rigidity through the corresponding acoustic tensor [20]. From the bulk K and shear G moduli, we obtain the indentation modulus $M = 4G(3K + G)/(3K + 4G)$ (for a homogeneous isotropic material) [5].

Nanoindentation has been used to measure the mechanical properties of C-S-H at the submicron scale [5]. The experiments consisted of probing the sample surface at different locations, with a needle of diameter ≈ 100 nm. The indentation modulus M and the hardness H are measured directly for each location, while the local packing fraction ϕ_0 is inferred by a self-consistent analysis. Figure 2 shows the indentation modulus from our present

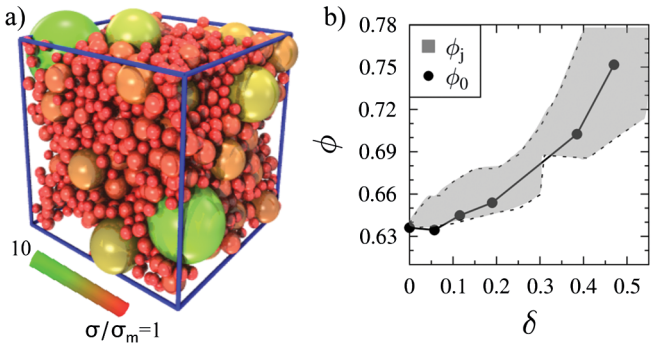

FIG. 1 (color online). (a) Snapshot of a simulated nanostructure with $\delta = 0.47$. The color code highlights the particle sizes (from small dark-red to large light-green ones). (b) Packing fraction ϕ_0 as a function of polydispersity δ; the shaded region corresponds to the range of jamming volume fractions for polydisperse hard spheres from Ref. [18]. Our results are averaged over 3–4 samples [16]. Error bars are within the marker symbol sizes. The lines are to guide the eye.

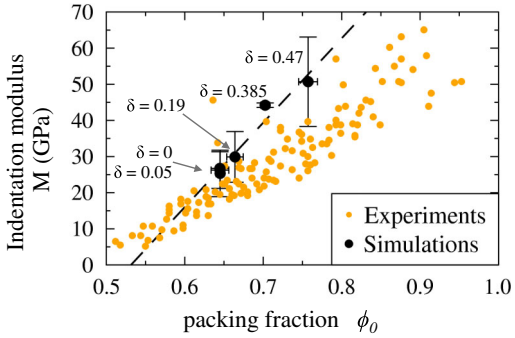

FIG. 2 (color online). Simulations at zero pressure and experiments from Ref. [11]. The dashed line interpolates our simulation results.

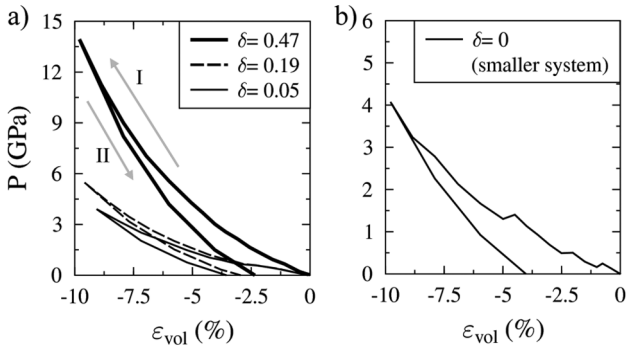

FIG. 3. Simulations of isotropic compression (stage I) and unloading (stage II). (a) Hysteresis on systems with N particles and different polydispersities ($\delta = 0.05$, $N = 1913$; $\delta = 0.19$, $N = 4548$; $\delta = 0.47$, $N = 1070$). (b) Strain discontinuities during loading of a smaller system with $N = 316$.

study at five packing fractions and their corresponding δ values. Also shown are the experimental data on the C-S-H phase in a white cement paste specimen [5,11].

The experiments indicated that within the same sample of C-S-H, the packing fraction ϕ_0 varied significantly with location. ϕ_0 ranges between 0.5 and 1, clustering between 0.6 and 0.8. M increases linearly with ϕ_0, and extrapolates to zero at $\phi_0 \sim 0.5$. We regard Fig. 2 as a reasonable validation of our attempt to describe the correlation between elastic rigidity and the packing fraction of C-S-H. Figure 1(b) provides the additional insight that in the present study a greater packing fraction, and correspondingly higher strength (see Fig. 2), entails larger polydispersity. This suggests a high degree of structural heterogeneity already at the submicron scale. It also indicates that the large fluctuations in local densities observed experimentally could be arising from large spatial variations of polydispersity of the C-S-H aggregates. Furthermore, because of size variation of the effective interactions, relatively soft domains can exist within stiffer regions. Such soft domains would consist of smaller particles, which are much more liable to local rearrangements, while the strongly cohesive large particles constitute the high stiffness backbone of the microstructure.

Figure 3(a) shows pressure-strain curves obtained by isotropic compression of the systems: from the reference state ($P = 0$) to a volume strain of $\varepsilon_{vol} = -10\%$ ($P > 0$), and then reversing back the strain loading to reach $P = 0$. All the curves show a significant hysteresis, indicating a plastic behavior which we consider related with the creep observed in nanoindentation experiments [9]. The analysis of local response, performed on a subsystem and shown in Fig. 3(b), indicates that such plastic behavior can be associated with local irreversible events, abrupt intermittent yielding (strain changes). These may be seen as the analogue of discrete deformations characteristic of nanoscale strain localization in atomistic simulations [21]. Experimentally, serrated flows in metallic glasses observed by *in situ* atomic emission monitoring have been linked to the initiation of shear bands [22]. We also observe that polydispersity tends to suppress serration behavior and, therefore, strain localization, which is consistent with reaching higher stresses at the same compression strain. An explanation is that the less mobile large particles in polydisperse systems can act as hard inclusions blocking the avalanche of irreversible displacements. We therefore expect that the behavior under large deformations should be affected by the PSD even at a fixed packing fraction, differently from the elastic moduli which we observe depend only on the packing fraction.

Our simple model brings out a physical picture of the structural and mechanical complexity of the C-S-H, which can help to resolve apparently contradicting observations. The microstructure of C-S-H displays indeed different characteristics when probed by different experimental techniques. Small-angle neutron scattering suggests C-S-H has a continuous gel-like structure with long range spatial correlations [8]. Various experimental techniques indicate the presence of nanocrystals with 1–10 nm size, with a disordered mesoscale organization [3,8,23,24]. On the other hand, nanoindentation, sampling spatial regions of order 100 nm, detects rather granular features of this solid [5,9]. It is conceivable that the three interpretations are parts of the same picture and, in fact, all these structural characteristics are resolved in the microstructure seen in high-resolution transmission electron microscopy images [24,25]. This multidomain character of the C-S-H microstructure is reflected in our model, where the attractive strength ϵ scales as the particle volume σ^3. Polydispersity hence can account for the presence of harder nanocrystalline regions embedded into a disordered softer matrix with similar chemical composition. Weak interactions in the matrix of small particles allow thermal motions to be important, which may give rise to the features of a relatively soft gel. On the other hand, the highly cohesive network of large inclusions causes the granular type of mechanical response.

Returning to the correlation between the packing fraction ϕ_0 and polydispersity, in our model we included attractive interactions, structural relaxation, and a finite

precipitation rate R_p, which go beyond packing of hard spheres. We have shown the resulting PSDs depend sensitively on R_p, although ϕ_0 and specific cohesive energy do not. Our interpretation is that the attractive interactions and the relaxation to zero pressure improve the efficiency and robustness of the packing, consistent also with the packing fraction of hard spheres with a potential-based protocol [10]. In fact our algorithm always approaches the random close packing for monodisperse systems [see Fig. 1(b)]. This synergistic effect of statics and dynamics on packing of cohesive media can be subtle and novel.

Several aspects of this work can benefit from refinements and extensions. We have thus far assumed the C-S-H particles are spherical but recent experiments suggest a platelet shape [26]. Ellipsoidal shapes can lead to a higher packing fraction, because of a larger number of possible particle contacts [27], but the coupled effect of shape and polydispersity remains to be studied. We anticipate the relation between the packing fraction and elastic properties (see Fig. 2) to depend more strongly on polydispersity than on particle shape, because of the $\varepsilon(\sigma) \sim \sigma^3$ scaling. Nevertheless, significant particle shape effects may emerge at large strain and with respect to failure mechanisms. Heterogeneous growth from unhydrated cement grain surfaces and a variable ionic solution may contribute to the experimentally measured spatial variety of the C-S-H packing fraction [28], and can also be considered in our model [16]. Finally, we note that cement setting belongs to a class of materials aging phenomena associated with slowly evolving structures. Irreversible deformation and viscoelastic response are manifestations of metastable equilibrium states that our discrete modeling approach can investigate systematically. Dynamical features such as glass rheology, creep deformation, and stress corrosion cracking [29,30], point to a new physical perspective for a broad appreciation of cement research.

This work is supported by Schlumberger (SDR Cambridge, U.S./SRPC Clamart, France) and by the CSHub at MIT. E. D. G. is supported by the SNSF (Grant No. PP00P2_126483/1).

[1] J. W. Bullard, H. M. Jennings, R. A. Livingston, A. Nonat, G. W. Scherer, J. S. Schweitzer, K. L. Scrivener, and J. J. Thomas, Cem. Concr. Res. **41**, 1208 (2011).
[2] A. Boumiz, C. Vernet, and F. C. Tenoudji, Adv. Cem. Bas. Mat. **3**, 94 (1996); J. J. Thomas, J. J. Biernacki, J. W. Bullard, S. Bishnoi, J. S. Dolado, G. W. Scherer, and A. Luttge, Cem. Concr. Res. **41**, 1257 (2011).
[3] H. M. Jennings, Cem. Concr. Res. **30**, 101 (2000).
[4] G. W. Scherer, Cem. Concr. Res. **29**, 1149 (1999).
[5] G. Constantinides and F.-J. Ulm, J. Mech. Phys. Solids **55**, 64 (2007).
[6] V. Trappe, V. Prasad, L. Cipelletti, P. N. Segre, and D. A. Weitz, Nature (London) **411**, 772 (2001).
[7] E. Del Gado, A. Fierro, L. de Arcangelis, and A. Coniglio, Phys. Rev. E **69**, 051103 (2004).
[8] A. J. Allen, J. J. Thomas, and H. M. Jennings, Nature Mater. **6**, 311 (2007).
[9] M. Vandamme and F.-J. Ulm, Proc. Natl. Acad. Sci. U.S.A. **106**, 10 552 (2009).
[10] C. Voivret, F. Radjaï, J-Y. Delenne, and M. S. El Youssoufi, Phys. Rev. E **76**, 021301 (2007).
[11] R. J. M. Pellenq, A. Kushima, R. Shasavari, K. J. Van Vliet, M. J. Buehler, S. Yip, and F.-J. Ulm, Proc. Natl. Acad. Sci. U.S.A. **106**, 16102 (2009).
[12] A. Zaccone, H. Wu, and E. Del Gado, Phys. Rev. Lett. **103**, 208301 (2009).
[13] H. Manzano, S. Moeini, F. Marinelli, A. C. T. van Duin, F.-J. Ulm, and R. J.-M. Pellenq, J. Am. Chem. Soc. **134**, 2208 (2012).
[14] ϵ_{ij} is obtained from Y with a harmonic approximation, i.e., considering d^2U_{ij}/dr_{ij}^2 for $r_{ij} = r_m$ equal to $Y\bar{\sigma}_{ij}$.
[15] The dimensionless temperature $T^* = k_B T/\varepsilon(\bar{\sigma}_{ij})$, at $T =$ 298 K, is $T^*(\bar{\sigma}_{ij} = 1\ \text{nm}) = 2.25 \times 10^{-2}$.
[16] See Supplemental Material at http://link.aps.org/supplemental/10.1103/PhysRevLett.109.155503 for details regarding the space-filling algorithm and the particle size distributions.
[17] H. J. H. Brouwers, Phys. Rev. E **74**, 031309 (2006).
[18] M. Hermes and M. Dijkstra, Europhys. Lett. **89**, 38005 (2010).
[19] J. F. Lutsko, J. Appl. Phys. **65**, 2991 (1989); We also cross-check the values of the bulk K and shear G moduli using a finite strain approach, obtaining good agreement.
[20] J. A. Ortega, F.-J. Ulm, and Y. Abousleiman, Geophys. Res. Lett. **74**, D65 (2009); The largest eigenvalue of the acoustic tensor is the longitudinal wave velocity. For our systems it is ~constant in each direction, with negligible polarization, indicating isotropy.
[21] S. Yip, J. Stat. Phys. **125**, 1109 (2006).
[22] D. Klaumünzer, A. Lazarev, R. Maaß, F. H. D. Torre, A. Vinogradov, and J. F. Löffler, Phys. Rev. Lett. **107**, 185502 (2011); P. Schall, D. Weitz, and F. Spaepen, Science **318**, 1895 (2007).
[23] R. González-Teresa, V. Morales-Florez, H. Manzano, and J. S. Dolado, Materiales de construccion **60**, 298 (2010); L. B. Skinner, S. R. Chae, C. J. Benmore, H. R. Wenk, and P. J. M. Monteiro, Phys. Rev. Lett. **104**, 195502 (2010); T. Mazumdar, S. Mazumder, and D. Sen, Phys. Rev. B **83**, 104302 (2011).
[24] Z. Xu and D. Viehland, Phys. Rev. Lett. **77**, 952 (1996).
[25] A. Barronet and O. Grauby (private communication).
[26] S. Garrault, E. Finot, E. Lesniewska, and A. Nonat, Mater. Struct. **38**, 435 (2005); W. S. Chiang, E. Fratini, P. Baglioni, D. Liu, and S. H. Chen, J. Phys. Chem. C **116**, 5055 (2012).
[27] A. Donev, I. Cisse, D. Sachs, E. A. Variano, F. H. Stillinger, R. Connelly, S. Torquato, and P. M. Chaikin, Science **303**, 990 (2004); S. Torquato, Rev. Mod. Phys. **82**, 2633 (2010); R. M. Baram and P. G. Lind, Phys. Rev. E **85**, 041301 (2012).
[28] M. Vandamme, F.-J. Ulm, and P. Fonollosa, Cem. Concr. Res. **40**, 14 (2010).
[29] Stress corrosion cracking, typical of metals, is analogous to coupled chemical degradation—fracture in cement.
[30] A. Kushima, J. Eapen, J. Li, S. Yip, and T. Zhu, Eur. Phys. J. B **82**, 271 (2011).